Time-Domain Measurements of Nanomagnet Dynamics Driven by Spin-Transfer Torques

I. N. Krivorotov,* N. C. Emley, J. C. Sankey, S. I. Kiselev, D. C. Ralph, R. A. Buhrman

We present time-resolved measurements of gigahertz-scale magnetic dynamics caused by torque from a spin-polarized current. By working in the time domain, we determined the motion of the magnetic moment throughout the process of spin-transfer–driven switching, and we measured turn-on times of steady-state precessional modes. Time-resolved studies of magnetic relaxation allow for the direct measurement of magnetic damping in a nanomagnet and prove that this damping can be controlled electrically using spin-polarized currents.

Spin-polarized electrons traversing a ferromagnet can transfer spin-angular momentum to the local magnetization, thereby applying a torque that may produce magnetic reversal or steady-state precession (*1*, *2*). This spin-transfer mechanism allows nanomagnets to be manipulated without magnetic fields, and it is the subject of extensive research for applications in nonvolatile memory, programmable logic, and microwave oscillators (*3*–*11*). However, the gigahertz-scale magnetic dynamics that can be driven by spin transfer have previously been measured using only frequency-domain techniques (*12*–*16*). Here we report direct time-resolved studies of dynamics excited by spin-transfer torques. By working in the time domain, we are able to characterize the full time-dependent magnetic response to pulses of spin-polarized currents, including transient dynamics. These measurements allow a direct view of the process of spin-transfer–driven magnetic reversal, and they determine the possible operating speeds for practical spin-transfer devices. The results provide rigorous tests of theoretical models for spin transfer (*1*, *9*, *17*–*19*) and strongly support the spin-torque model (*1*, *18*) over competing theories that invoke magnetic heating (*9*, *20*).

We studied nanopillar-shaped samples consisting of two 4-nm-thick permalloy (Py ≡ $Ni_{80}Fe_{20}$) ferromagnetic layers separated by an 8-nm-thick Cu spacer layer (Fig. 1A, inset). Both Py layers and the Cu spacer were etched to have an elliptical area of approximately 130 × 60 nm. Current flows perpendicular to the layers through Cu electrodes. The relative angle between the magnetic moments of the Py layers was detected by changes in the sample resistance due to the giant magnetoresistance effect. For time-resolved measurements on subnanosecond scales, signal-to-noise considerations require averaging over multiple signal traces. If the signal is oscillatory, the phase of the oscillations has to be the same in each trace or else the signal will be lost in averaging (*21*). This requires that the samples be engineered so that the initial (equilibrium) angle between the magnetic moments of the two layers, θ_0, is different from zero and is well controlled. Our devices were specially designed to provide this control. The equilibrium orientation of our top free-layer Py moment was governed primarily by the shape anisotropy of the elliptical device. We exchange-biased the bottom layer at an angle of 45° to the top layer easy axis using an 8-nm-thick antiferromagnetic $Ir_{20}Mn_{80}$ underlayer. From the combined effects of exchange biasing, shape anisotropy, and the interlayer dipole interaction, we estimated that $\theta_0 \approx 30°$. The existence of a nonzero equilibrium angle was reflected in the nonmonotonic dependence of the sample resistance (R) on magnetic field applied along the exchange bias direction (Fig. 1A for sample 1). To minimize thermal fluctuations of the initial magnetic-moment angles, we worked at low temperature (≤40 K) in a variable-temperature probe station.

The dependence of R on bias current I was similar to results from previous experiments (*7*, *13*). For magnetic field H less than the coercive field H_c of the free layer, spin transfer from I drives hysteretic switching of

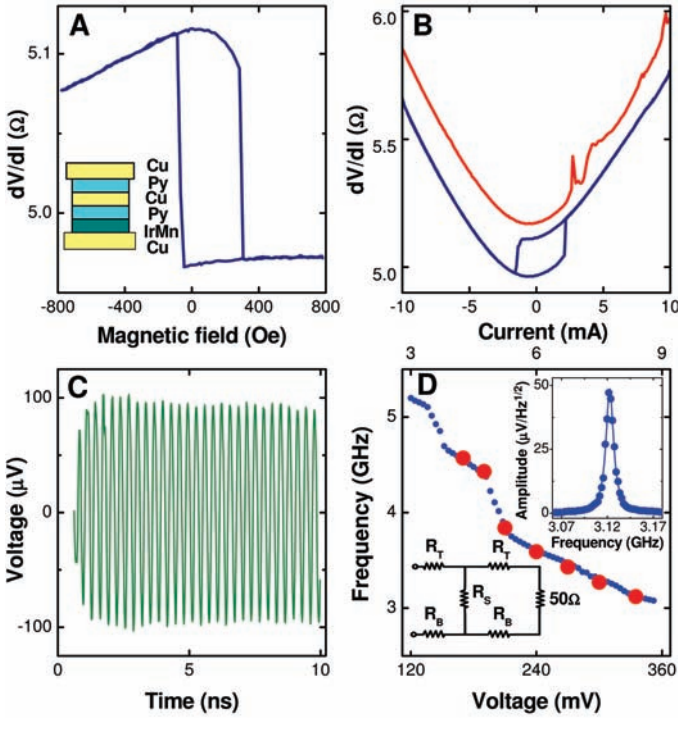

Fig. 1. Data for sample 1. (**A**) Resistance, measured in a four-point configuration, as a function of magnetic field applied along the exchange-bias direction at T = 40 K. (Inset) Composition of the sample. (**B**) Resistance as a function of current at $H = 0$ (blue line) and 700 Oe (red line, offset by 0.2 ohm). (**C**) Oscillatory voltage generated by precessional motion of the free magnet in response to a 335-mV dc voltage step applied to the device at H = 630 Oe. The data were obtained by averaging over 2 × 10^4 oscilloscope traces using the analysis described in (*23*). The start time corresponding to the midpoint of the applied bias step is t = 0.3 ns. The precessional dynamics exhibit a subnanosecond turn-on time and a long dephasing time (~10^2 ns). (**D**) Variation of the precessional frequency measured in the frequency domain with a dc bias current (blue circles, top scale) and measured in the time domain with a fast voltage step (red circles, bottom scale). (Upper inset) Frequency-domain measurement of the voltage spectrum for a dc bias I = 8.4 mA, equivalent to the voltage step amplitude in (C). (Lower inset) Equivalent circuit seen by the incident voltage step, with sample resistance R_S = 5 ohm, top contact resistances R_T = 10 ohm, bottom contact resistances R_B = 7 ohm, and the 50-ohm connection to the sampling oscilloscope.

Cornell University, Ithaca, NY 14853, USA.

*To whom correspondence should be addressed. E-mail: ink3@cornell.edu

the free layer, and for $H > H_c$, nonhysteretic peaks and shoulders appear in the differential resistance dV/dI (Fig. 1B). Positive current corresponds to electrons flowing from the free to the pinned magnet. Frequency-domain measurements made using a spectrum analyzer demonstrate that the nonhysteretic features are associated with the turning on and off of dynamical magnetic modes and that precessional dynamics can also precede switching for $H < H_c$ (*13*, *14*, *22*).

For time-resolved measurements of spin-transfer–driven dynamics, we applied voltage steps with 65-ps rise times using a 50-GHz probe, causing steps of current through the device. Starting with the two magnetic moments in the low-resistance configuration ($\theta_0 < 90°$), steps of positive polarity applied a torque, which rotated the free-layer moment away from the fixed-layer moment and, consequently, excited free-layer dynamics (*1*, *7*). We monitored the voltage across the device with another 50-GHz probe connected to a 12-GHz sampling oscilloscope through a 25-dB amplifier. The measured signal is the sum of a voltage step transmitted through the device and an oscillatory signal due to magnetic dynamics. The signal caused by magnetic dynamics was determined by a background-subtraction procedure (*23*).

Figure 1C shows the magnetic-dynamics component of the transmitted voltage for a 335-mV incident step at H = 630 Oe. A strong oscillatory signal is seen at 3.12 GHz. This frequency increases with H as expected for a signal due to precession of magnetic moment in a field and decreases with increasing amplitude of the voltage step. A similar dependence of the steady-state precession frequency on field and dc current is found in frequency-domain measurements, so we can calibrate our current step amplitudes by comparing the two types of experiments (Fig. 1D). [Discontinuities in Fig. 1D are related to transitions between precessional modes (*15*)]. The conversion factor between the incident voltage amplitude and the current through the sample is 0.025 ohm^{-1}. This calibration agrees with the equivalent circuit for our apparatus (Fig. 1D, inset) to within 5%.

The amplitude of the oscillatory signal in Fig. 1C increases from zero to a maximum over a subnanosecond time interval, followed by a slow decay. Because frequency-domain measurements show that the motion at long times is a steady-state precessional mode, the decay should not be understood as an actual loss of precession amplitude. Instead, it is an effect of averaging over multiple traces that do not maintain phase coherence. The measured dephasing rate (~10 MHz) corresponds well to the width of the spectral peak in the frequency domain at the equivalent dc bias (Fig. 1D, inset). For the bias conditions of Fig. 1, C and D (inset), the amplitudes of the signals in both the time- and frequency-domain measurements are consistent with a maximum precession angle of approximately 35° (*23*).

The turn-on time of the oscillations (<1 ns) in Fig. 1C is much faster than the dynamics excited in samples for which the moments of the two magnetic layers are initially approximately parallel (*21*). This confirms simulations showing that an increasing offset angle θ_0 should reduce this response time (*18*, *24*).

At $H < H_c$, spin transfer can drive magnetic reversal. The dynamical process by which reversal is achieved has been a subject of considerable theoretical debate. Some models (*1*, *18*) predict that the transfer of angular momentum can generate precession in a nanomagnet with a precession angle that increases continuously until the moment has flipped. Other models (*9*, *20*) have suggested that spin transfer excites short-wavelength magnons, effectively heating the sample incoherently to accelerate reversal. Our time-domain techniques enabled us to observe directly the dynamics throughout the process of spin-transfer–driven reversal, and we found that reversal on nanosecond scales was accomplished by a process of precession. For this measurement, we applied two pulse sequences (signal and baseline) at H = 0 Oe (*21*). For the signal sequence, we began with the two magnetic moments in the low-resistance state and then applied a 10-ns current pulse of positive polarity, followed by a 100-ns reset current pulse of negative polarity and a 10-μs waiting time at zero bias. The nanomagnet switched from the low- to the high-resistance state during the positive-going pulse of this sequence and was returned to the low-resistance state by the reset pulse. To obtain a baseline signal for subtracting the transmitted voltage pulse, we started with the moments in the high-resistance configuration and applied only 10-ns pulses of positive polarity, so that the moments always remained in the high-resistance state.

The signal-minus-baseline traces are shown in Fig. 2, A to C, for three magnitudes of the current pulse. The initial voltage drop V is due to the pulse onset at time $t \approx 0.3$ ns. After the pulse onset, coherent oscillations are present, which lead to an increase in V that corresponds to reversal from the low- to high-resistance magnetic configuration. The transition between the two resistance states in Fig. 2, A to C, appears to be gradual. However, we argue that this apparent gradualness can be explained by averaging over multiple switching events, each with a sharp transition but with a distribution of initial magnetic-orientation angles due to thermal fluctuations and possibly different initial micromagnetic configurations (*25*). Figure 2D shows the results of a simulation of current-induced nanomagnet switching performed by numerical solution of the Landau-Lifshitz-Gilbert (LLG) equation of motion, including the Slonczewski form of the spin-transfer torque (*26*), solved in the approximation that the nanomagnet responds as a single macrospin. The blue line in Fig. 2D shows the calculated voltage trace for an individual

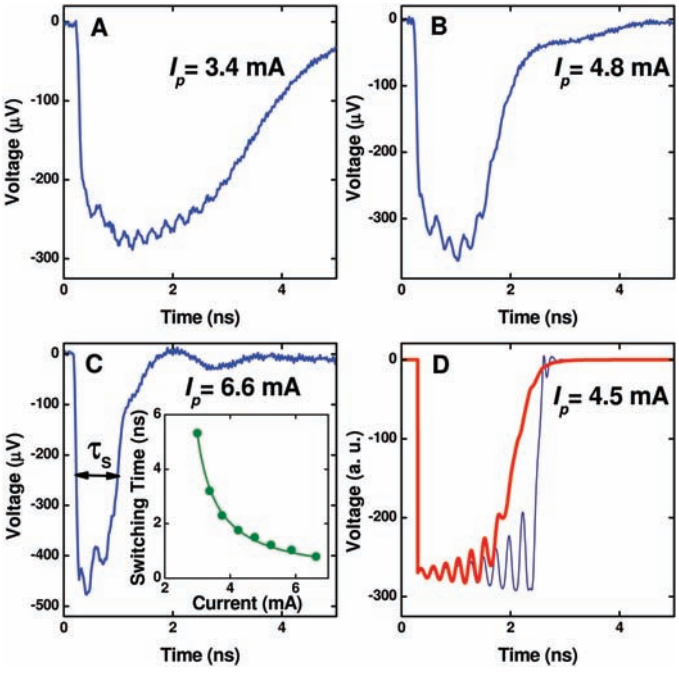

Fig. 2. Voltage signals due to current-induced switching of the free-layer magnet in sample 1 at H = 0 Oe and T = 40 K, during a 10-ns current pulse of three different amplitudes: (**A**) I_p = 3.4 mA, (**B**) I_p = 4.8 mA, and (**C**) I_p = 6.6 mA. Each plot represents an average over 4 × 10^4 oscilloscope traces. [Inset in (C)] Dependence of switching time on I_p, with a fit to $\tau_S = \tau_A/(I_p/I_0 - 1)$. (**D**) Voltage signals given by LLG simulations of current-induced switching, assuming $\mu_0 M_S$ = 0.81 T for Py, a damping parameter α = 0.025, a current polarization P = 0.3, a uniaxial anisotropy field = 300 Oe, and a 30° angle between the magnetic moment of the free layer and the current polarization. The blue line shows an individual switching event. The red line is an average over 2000 switching events with a Gaussian distribution of initial directions for the magnetic moment equivalent to thermal fluctuations at 40 K. a.u., arbitrary units.

event of precessional reversal. The red line is an average over 2000 switching events for a Gaussian distribution of the initial angle for the moment of the free magnet. We assume a standard deviation of 4°, corresponding to the thermal fluctuations at temperature $T = 40$ K for a nanomagnet with the uniaxial anisotropy energy of 0.8 eV. Given the quality of agreement between the simulations and the data in Fig. 2, A to C, we conclude that phase-coherent precessional motion within the spin-torque model gives a good description of the current-induced switching process.

We define the switching time τ_S as the interval between the pulse onset and the midpoint of the transition between the two resistance states. The dependence of τ_S on the amplitude of the current pulse I_p is plotted in the inset of Fig. 2C. The data are fit well by the expression $\tau_S = \tau_A/(I_p/I_0 - 1)$ predicted by LLG simulations of spin-torque–induced reversal (*18*), with the zero-temperature critical current for nanomagnet switching $I_0 = 2.37 \pm 0.03$ mA and $\tau_A = 1.39 \pm 0.06$ ns, where τ_A is a fitting parameter.

One of the fundamental predictions of the spin-torque model is that small applied spin-polarized currents should modify the effective magnetization-damping parameter α' of a nanomagnet (*1*). According to this model, the spin-transfer torque has a large component that is colinear with the Gilbert damping torque. Therefore, the spin torque can act to enhance or reduce the effective damping, depending on the sign of I. At the critical current for the onset of dynamical states, the effective damping is expected to go to zero for small-angle excitations. This prediction has not been tested previously because the damping parameter cannot be determined from frequency-domain spectra such as those shown in Fig. 1D. However, by exciting the free-layer moment to a nonequilibrium angle and watching in the time domain as it relaxes to equilibrium, we can directly measure the effective magnetic damping as a function of I.

The minimum current required to excite magnetic dynamics at $H = 0$ Oe for sample 2 is $I_D = 1.25 \pm 0.05$ mA, based on frequency-domain measurements of the microwave signal emitted by the precessing magnet under dc bias (Fig. 3A). To measure the dependence on I of the decay time for magnetic relaxation, τ_d, and thus of the effective damping α', we began with the device in the low-resistance state at $H = 0$ Oe, biased it with a subcritical ($I \leq I_D$) positive dc current, and then applied a positive 3-mA 650-ps pulse. From measurements such as those shown in Fig. 2, A to C, we determined that this short pulse rotates the free-layer magnetic moment away from its equilibrium direction but does not produce magnetic reversal. Therefore, after the falling edge of the pulse, the moment relaxes back to equilibrium by magnetic precession with a decreasing amplitude, producing (because of the current bias) a decaying oscillatory voltage. For background determination, we repeated the measurement with the sample initially in the high-resistance configuration and subtracted the result from the signal traces. Figure 3B shows the magnetic relaxation signal for a 0.6-mA dc bias current. By fitting to an exponentially decaying sine function, we determined a relaxation time of 0.85 ns. This is much shorter than the dephasing time for the regime of steady-state precession, indicating that the decaying signal corresponds to an oscillation with decreasing amplitude rather than a loss of phase coherence. As we increased I toward I_D, the relaxation time grew markedly (Fig. 3C). In Fig. 3D, we summarize the results for several values of I in terms of the effective damping parameter $\alpha' = 2/(\tau_d \gamma \mu_0 M_S)$ (*27*), where γ is the gyromagnetic ratio, μ_0 is the magnetic permeability of free space, M_S is the free-layer magnetization, and $\mu_0 M_S = 0.81$ T as measured by superconducting quantum interference device (SQUID) magnetometry for a 4-nm Py film. The damping exhibits an approximately linear decrease with increasing I, extrapolating to zero near I_D, in excellent agreement with the prediction of the spin-torque model (*1*, *18*). The measured damping does not go to zero precisely at I_D, probably because our measurements involve tipping angles that are larger than the steady-state precession angle for the dynamical modes at I just above I_D. If we extrapolate the measured effective damping to $I = 0$, we estimate the damping parameter of the free magnet to be $\alpha = 0.025$, larger than the value $\alpha = 0.007$ obtained from ferromagnetic resonance measurements of a 3-nm-thick Py film between Cu layers (*28*). Our larger value may be due to spin pumping between the two magnetic layers in our device (*29*, *30*) and/or edge effects at the boundary of the nanopillar.

Our time-resolved measurements have important implications both for the theoretical understanding of spin-transfer torques and for potential applications. All of our data are in excellent agreement with the predictions of the Slonczewski spin-torque model (*1*): that spin transfer can reduce the effective magnetic damping for applied currents less than a critical current and, at higher currents, can drive phase-coherent precessional magnetic dynamics. The measurements are not consistent with models in which the dominant spin-transfer mechanism is incoherent magnon excitation equivalent to effective heating (*9*, *20*). Spin transfer can drive magnetic reversal by precession, with switching times that are less than 1 ns and exhibit narrow statistical distributions, which are very promising characteristics for magnetic-memory applications. For larger applied magnetic fields, the steady-state precessional modes produced by spin transfer can have short turn-on times (<1 ns) and long decoherence times ($\sim 10^2$ ns), which are appropriate for applications in high-speed signal processing.

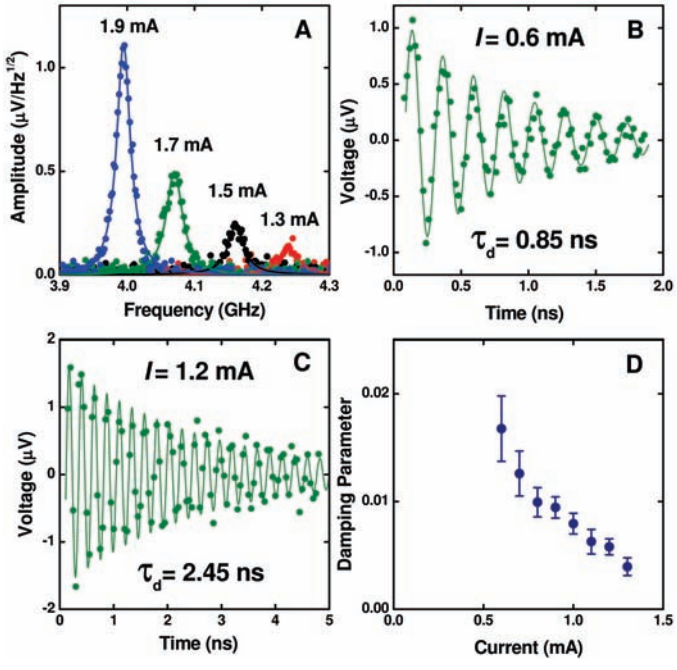

Fig. 3. Data for sample 2. (**A**) Frequency spectra of magnetic precession signals that are generated under different dc current biases at $H = 0$ Oe and $T = 7$ K. The extrapolated critical current for the onset of precessional dynamics is $I_D = 1.25 \pm 0.05$ mA. (**B** and **C**) Signals generated by a free decay of the nanomagnet to its equilibrium direction in the presence of currents $I < I_D$: (B) $I = 0.6$ mA and (C) $I = 1.2$ mA. The data in (B) and (C) were obtained by averaging over 10^6 oscilloscope traces. The start time corresponding to the midpoint of the step to the final current value is $t = -0.1$ ns. The lines are fits to exponentially decaying sinusoid functions. (**D**) Dependence of the effective damping parameter α' on dc bias current. Error bars indicate the 68% confidence limits obtained from the least-squares fit to the oscillatory decay data such as shown in (B) and (C).

References and Notes

1. J. C. Slonczewski, *J. Magn. Magn. Mater.* **159**, L1 (1996).
2. L. Berger, *Phys. Rev. B* **54**, 9353 (1996).
3. M. Tsoi *et al.*, *Phys. Rev. Lett.* **80**, 4281 (1998) and erratum, *Phys. Rev. Lett.* **81**, 493(E) (1998).

4. E. B. Myers, D. C. Ralph, J. A. Katine, R. N. Louie, R. A. Buhrman, *Science* **285**, 867 (1999).
5. J.-E. Wegrowe, D. Kelly, Y. Jaccard, P. Guittienne, J.-P. Ansermet, *Europhys. Lett.* **45**, 626 (1999).
6. J. Z. Sun, *J. Magn. Magn. Mater.* **202**, 157 (1999).
7. J. A. Katine, F. J. Albert, R. A. Buhrman, E. B. Myers, D. C. Ralph, *Phys. Rev. Lett.* **84**, 3149 (2000).
8. J. Grollier *et al.*, *Appl. Phys. Lett.* **78**, 3663 (2001).
9. S. Urazhdin, N. O. Birge, W. P. Pratt Jr., J. Bass, *Phys. Rev. Lett.* **91**, 146803 (2003).
10. B. Özyilmaz *et al.*, *Phys. Rev. Lett.* **91**, 067203 (2003).
11. M. R. Pufall *et al.*, *Phys. Rev. B* **69**, 214409 (2004).
12. M. Tsoi *et al.*, *Nature* **406**, 46 (2000).
13. S. I. Kiselev *et al.*, *Nature* **425**, 380 (2003).
14. W. H. Rippard, M. R. Pufall, S. Kaka, S. E. Russek, T. J. Silva, *Phys. Rev. Lett.* **92**, 027201 (2004).
15. S. I. Kiselev *et al.*, *Phys. Rev. Lett.* **93**, 036601 (2004).
16. M. Covington, M. AlHajDarwish, Y. Ding, N. J. Gokemeijer, M. A. Seigler, *Phys. Rev. B* **69**, 184406 (2004).
17. Y. B. Bazaliy, B. A. Jones, S. C. Zhang, *Phys. Rev. B* **57**, 3213 (1998).
18. J. Z. Sun, *Phys. Rev. B* **62**, 570 (2000).
19. M. D. Stiles, A. Zangwill, *Phys. Rev. B* **65**, 014407 (2002).
20. A. Fabian *et al.*, *Phys. Rev. Lett.* **91**, 257209 (2003).
21. R. H. Koch, J. A. Katine, J. Z. Sun, *Phys. Rev. Lett.* **92**, 088302 (2004).
22. I. N. Krivorotov *et al.*, *Phys. Rev. Lett.* **93**, 166603 (2004).
23. Materials and methods are available as supporting material on *Science* Online.
24. X. Zhu, J.-G. Zhu, *J. Appl. Phys.* **95**, 7318 (2004).
25. J. Miltat, G. Albuquerque, A. Thiaville, C. Vouille, *J. Appl. Phys.* **89**, 6982 (2001).
26. J. C. Slonczewski, *J. Magn. Magn. Mater.* **247**, 324 (2002).
27. R. H. Koch *et al.*, *Phys. Rev. Lett.* **81**, 4512 (1998).
28. S. Mizukami, Y. Ando, T. Miyazaki, *Phys. Rev. B* **66**, 104413 (2002).
29. Y. Tserkovnyak, A. Brataas, G. E. W. Bauer, *Phys. Rev. B* **67**, 140404 (2003).
30. B. Heinrich *et al.*, *Phys. Rev. Lett.* **90**, 187601 (2003).

31. We acknowledge support from the Defense Advanced Research Projects Agency through Motorola; from the Army Research Office; and from the NSF/Nanoscale Science and Engineering Center program through the Cornell NanoScale Facility/National Nanotechnology Infrastructure Network. We also acknowledge NSF support through use of the Cornell Nanofabrication Facility/National Nanotechnology Infrastructure Network and the Cornell Center for Materials Research facilities.

Supporting Online Material
www.sciencemag.org/cgi/content/full/307/5707/228/DC1
Materials and Methods
Fig. S1
References

28 September 2004; accepted 24 November 2004
10.1126/science.1105722

Al Cluster Superatoms as Halogens in Polyhalides and as Alkaline Earths in Iodide Salts

D. E. Bergeron,[1] P. J. Roach,[1] A. W. Castleman Jr.,[1]* N. O. Jones,[2] S. N. Khanna[2]

Two classes of gas-phase aluminum-iodine clusters have been identified whose stability and reactivity can be understood in terms of the spherical shell jellium model. Experimental reactivity studies show that the $Al_{13}I_x^-$ clusters exhibit pronounced stability for even numbers of I atoms. Theoretical investigations reveal that the enhanced stability is associated with complementary pairs of I atoms occupying the on-top sites on the opposing Al atoms of the Al_{13}^- core. We also report the existence of another series, $Al_{14}I_x^-$, that exhibits stability for odd numbers of I atoms. This series can be described as consisting of an $Al_{14}I_3^-$ core upon which the I atoms occupy on-top locations around the Al atoms. The potential synthetic utility of superatom chemistry built upon these motifs is addressed.

The electronic properties and chemical reactivity of small metal clusters can be fundamentally different from bulk metals, which are well described by band theory, and compounds with only a few metal atoms, where bond formation and charge states typically lead to stable atomic shells for each atom. For clusters of free-electron metals, a model is commonly used in which the nuclei and innermost electrons form a positively charged core with an essentially uniform potential. All of the valence electrons from the individual atoms in the cluster are then subjected to this potential, and the jellium electronic shell structure emerges with stable configurations of electrons (2, 8, 18, 20,…) that differ from the atomic series (2, 10, 18,…) (*1*–*6*).

Such clusters could be described as superatoms, because clusters of a given element can have chemical and electronic properties resembling those of another atom; hence, superatoms can be regarded as an extension of the periodic table to a third dimension (*1*–*23*). Similar principles have been discussed for the description of the properties of various functional groups in synthetic chemistry, particularly Grimm's hydrogen-displacement theorem (pseudoelements) and Haas' concept of paraelements (*24*).

We recently demonstrated that an Al_{13} cluster acts like a superhalogen even when combined with a conventional halogen, namely I, to form an $Al_{13}I^-$ cluster compound (*22*, *23*). Through reactivity studies of Al_nI^- clusters combined with state-of-the-art ab initio calculations, we find that $Al_{13}I^-$ is a remarkably stable species and that the extra electron charge in $Al_{13}I^-$ is mostly localized at the Al_{13} unit.

Halogens form extended polyhalides in both the gas and condensed phases. For example, I forms polyiodides within the series I_{2n+1}^- that consist of I^- or I_3^- ions bound to I_2 molecules in the form of chains. As an example, the ground state of I_5^- is a V-shaped structure with two I_2 molecules coordinated to an apical iodide $[(I^-)\bullet 2I_2]$. Given that Al_{13}^- can act as a halide ion when coordinated to one or two I atoms, one would predict that interactions with I_2 molecules might lead to complex clusters with structures similar to I_{2n+1}^- polyiodides.

Herein, we present evidence of the formation of a previously unknown class of polyhalide-like molecules by replacing an I atom in traditional polyiodides with an Al_{13}^- cluster. Although it is possible to form $Al_{13}I_x^-$ clusters for all x, trends in reactivity reveal that members of this series are particularly stable when x is even. Because traditional interhalogen and polyhalide ions require an odd total number of halogen atoms, the $Al_{13}I_x^-$ clusters appear to resemble these known species. Our ab initio calculations, however, indicate that this apparent similarity is slightly deceptive and that the $Al_{13}I_{2x}^-$ clusters present an entirely different geometry with subtle differences in chemical behavior. Whereas polyiodides contain I_2 molecules, superpolyhalides only contain I atoms. Further, the stability of clusters with even numbers of I atoms has a completely different origin than the stability in conventional polyiodides.

We also show that Al_{14} can behave as an alkaline earth metal–like superatom. A second series of clusters of the type $Al_{14}I_x^-$ exhibits pronounced stability when x is odd. The series begins with $Al_{14}I_3^-$, in which the Al_{14} core behaves as a dication, and from our theoretical investigations we describe the mechanism by which larger members of the series build upon this core. The synthetic importance of these gas phase findings are underscored by recent results that show that the solution phase "metalloid" cluster compounds (*25*, *26*) synthesized by Schnöckel and co-workers are in fact, at their core, the same cluster species found in the gas phase (*27*, *28*).

The Al cluster anions react readily with I_2 (Fig. 1 and fig. S1), leading to a distribution of clusters of the type $Al_nI_x^-$ (*29*). Despite the addition of I_2, x need not be even. The addition of single I atoms might be partially attributed to the equilibrium of I_2 with atomic I in the vapor phase, but, as we describe in more detail

[1]Department of Chemistry and Department of Physics, Pennsylvania State University, University Park, PA 16802, USA. [2]Department of Physics, Virginia Commonwealth University, Richmond, VA 23284, USA.

*To whom correspondence should be addressed. E-mail: awc@psu.edu